On the importance of irreversibility of corrosion inhibitors for active coating protection of AA2024-T3

Visser, Peter; Terryn, H.; Mol, J. M.C.

DOI
10.1016/j.corsci.2018.05.037

Publication date
2018

Document Version
Final published version

Published in
Corrosion Science

Corrosion Science 140 (2018) 272–285

Contents lists available at ScienceDirect

Corrosion Science

journal homepage: www.elsevier.com/locate/corsci

On the importance of irreversibility of corrosion inhibitors for active coating protection of AA2024-T3

P. Visser[a,b,*], H. Terryn[a,c], J.M.C. Mol[a]

[a] Delft University of Technology, Department of Materials Science and Engineering, Mekelweg 2, 2628 CD, Delft, The Netherlands
[b] AkzoNobel, Rijksstraatweg 31, 2171AJ, Sassenheim, The Netherlands
[c] Vrije Universiteit Brussel, Research Group of Electrochemistry and Surface Engineering (SURF), Pleinlaan 2,1050, Brussels, Belgium

ARTICLE INFO

Keywords:
Aluminium
Lithium
Organic
Inhibitor
Reversibility
Active protection

ABSTRACT

Inhibitor leaching, fast, effective and irreversible passivation are essential for active protective coatings to protect aluminium alloys. This study presents the comparison of the active protective properties of lithium carbonate and two organic corrosion inhibitors, benzotriazole and 2-mercaptobenzothiazole, on aluminium alloy 2024-T3 with a special focus on the irreversibility of the inhibition. A combined approach of electrochemical measurements, optical observations, surface roughness and weight-loss measurements revealed the reversible inhibition behaviour of benzotriazole and 2-mercaptobenzothiazole on AA2024-T3. On the contrary, lithium carbonate demonstrated fast, effective and irreversible corrosion inhibition, providing the essential characteristics needed for effective active corrosion protection from coatings.

1. Introduction

Organic coatings loaded with corrosion inhibitors are widely used for the protection of aluminium structures [1]. The corrosion protection mechanism of these coatings is based on the release of corrosion inhibitors from the coating matrix. This active protective process, known as leaching, is initiated by the ingress of water via a defect or crack in the coating, enabling the dissolution and transport of the corrosion inhibitor to the defect to inhibit the corrosion process [2,3].

Aerospace aluminium alloys, such as AA2024-T3, are highly susceptible to localized corrosion in chloride-containing aqueous solutions due to the presence of copper-rich intermetallic particles in the alloy microstructure [4–6]. These intermetallic particles are known to act as active sites for the cathodic oxygen reduction reaction which enhance these localized corrosion phenomena [7]. The inhibition of the electrochemical processes at these intermetallic particles (i.e. suppressing the oxygen reduction reaction) has been an important strategy in the search for environmentally benign alternatives for the highly effective but toxic hexavalent chromium compounds [8].

Over the years many organic compounds have been evaluated for their corrosion inhibiting activity on aluminium substrates [9]. Especially, heterocyclic compounds such as benzotriazole (BTA) and 2-mercaptobenzothiazole (2-MBT) gained interest as potential corrosion inhibitors for aerospace aluminium alloys due to their copper-complexing characteristics [10,11]. Both corrosion inhibitors have demonstrated their ability to inhibit the oxygen reduction reaction at copper-rich cathodic intermetallic particles present in the alloys by the formation of an insoluble complex or a polymeric film via a physisorption or chemisorption mechanism providing a physical-chemical barrier for corrosive species [12–14]. These inhibitors are considered copper inhibitors but for aluminium alloys, BTA or 2-MBT have been reported as pure cathodic inhibitors covering the copper-rich intermetallic particles [12] or mixed inhibitors providing both anodic and cathodic inhibition covering the aluminium matrix as well [13,15]. Furthermore, Harvey et al. demonstrated that both BTA and 2-MBT are able to inhibit corrosion of AA2024-T3 and AA7075-T6 aluminium alloys with inhibitor efficiencies higher than 90% [16]. Based on these inhibitive properties, BTA and 2-MBT have received significant interest of the scientific community and their active corrosion inhibiting activity has been studied widely, in solution on AA2024-T3 [13,17] or an Al/Cu galvanic-coupling model system [18,19], in coatings [20–22] and various “smart coating” approaches using nano-containers [23–28], and poly-urea micro-capsules [29].

Since a few years, lithium-salts gained interest as a potential alternative for chromates as leaching corrosion inhibitor in organic coatings and demonstrated active protective properties on AA2024-T3 [30]. Lithium-salts demonstrated their viability as leachable corrosion inhibitor when incorporated in an industrial coating matrix in a direct comparison with a chromate inhibitor loaded coating system under industrial testing conditions [31]. It was demonstrated that lithium-

* Corresponding author at: Delft University of Technology, Department of Materials Science and Engineering, Mekelweg 2, 2628 CD, Delft, The Netherlands.
E-mail address: p.visser-1@tudelft.nl (P. Visser).

https://doi.org/10.1016/j.corsci.2018.05.037
Received 8 April 2018; Received in revised form 19 May 2018; Accepted 29 May 2018
Available online 30 May 2018
0010-938X/

salts are able to leach from an organic coating matrix and create alkaline conditions that promote the formation of a protective layer on the alloy in a coating defect and consequently inhibit corrosion effectively [32]. This layer is generated by a multistep conversion process of oxide thinning, anodic dissolution and a competitive growth and dissolution process resulting in an aluminium oxide/hydroxide layer with a three-layered morphology of dense, porous and columnar regions [33]. The corrosion protective properties of this layer can be attributed to the dense region at the aluminium/oxide interface [34].

While the aforementioned organic inhibitors as well as the Li-based inhibitor technology have been reported to provide significant corrosion protection to AA2024-T3, another pivotal criterion for effective active corrosion protection of these inhibitor types has not been studied in detail: the irreversibility of inhibition. Irreversibility of corrosion inhibitors can be defined as, the ability of a corrosion inhibitor to passivate the metal surface and once passivated, it retains its protective properties when the concentration of the corrosion inhibitor decreases. The irreversibility of the protective properties of a corrosion inhibitor are essential for long-term corrosion protection. Despite excellent corrosion inhibiting results with BTA at initial stage, Recloux et al. [13,15] reported that the inhibitor film stability of BTA seems to be dependent on the presence of inhibitor and Zheludkevich et al. [13] observed degradation of the BTA protective layer after 50 h exposure to the inhibitor solutions. These observations make it worthwhile to investigate the active protective properties and irreversibility of these well-known organic corrosion inhibitors in comparison to the new lithium carbonate (Li_2CO_3) inhibitor.

In this comparative study the active protective properties of Li_2CO_3 and the organic inhibitors BTA and 2-MBT on AA2024-T3 were investigated. The intrinsic corrosion protective properties of the inhibitors on AA2024-T3 were investigated using electrochemical impedance spectroscopy (EIS) and potentiodynamic polarization measurements. Furthermore, the corrosion inhibitors were incorporated in an organic model coating to evaluate their active corrosion protective properties by the measurement of inhibitor leaching from the coating matrix. The corrosion protective properties in a defect area of an artificially damaged coating were assessed by optical microscopy and with EIS after exposure to the neutral salt spray test. Complementary EIS, surface roughness and weight loss measurements were performed to study the reversibility and the inhibitor efficiency of the corrosion inhibitors. This combination of experimental approaches provided an enhanced insight into the mechanisms and robustness of the active corrosion inhibition provided by these corrosion inhibitors.

2. Experimental

2.1. Corrosion inhibition and inhibitor reversibility in an electrochemical cell

2.1.1. Materials and sample preparation

Aluminium alloy panels AA2024-T3 bare (5.0 × 7.0 cm, 0.8 mm thickness) were obtained from Arconic. Before the experiment, the panels were degreased with acetone to remove surface contaminations and abraded with Scotch-Brite™ 7447 PRO pads, rinsed with deionized water, and dried with compressed air.

The corrosion inhibitors were obtained from Sigma-Aldrich: benzotriazole (99%) (BTA), 2-mercaptobenzothiazole (2-MBT) (97%) and lithium carbonate (Li_2CO_3) (99.997%). The inhibitor solutions were prepared in an aqueous 0.05 M NaCl solution with the following concentrations: no inhibitor, 5 mM BTA, 5 mM Li_2CO_3 and 1 mM 2-MBT. Throughout the manuscript these solutions will be referred to as blank solution, BTA solution, Li_2CO_3 solution and 2-MBT solution, respectively. Preliminary experiments demonstrated that 5 mM was the minimum concentration needed to obtain reproducible corrosion inhibition with Li_2CO_3 and BTA. Due to the low solubility of this inhibitor in water, the concentration of the 2-MBT solution was limited to 1 mM. The solubility of the inhibitors is as follows: 2-MBT, 0.1 mM/100 ml [35], BTA 1.7 mM/100 ml [36] and Li_2CO_3: 17.5 mM/100 ml [37])

2.1.2. Electrochemical assessment of corrosion inhibition and inhibitor reversibility

2.1.2.1. Electrochemical impedance spectroscopy. The aluminium panels were installed in an electrochemical cell and exposed to solutions with and without corrosion inhibitor for 24 h. After this period, EIS spectra were recorded at the open circuit potential (OCP) using a Gamry Interface 1000 computer-controlled potentiostat. A three-electrode set-up was used, consisting of the aluminium sample as the working electrode (surface area 3.14 cm^2), platinum gauze counter electrode and a saturated calomel electrode (SCE) as reference electrode in a Faraday cage. The EIS measurements were performed over a frequency range from 10^{-2} Hz to $3{\cdot}10^4$ Hz, applying a 10 mV sinusoidal amplitude and performing 10 measurements per frequency decade. All measurements were performed at least in triplicate.

2.1.2.2. Potentiodynamic polarizations. Potentiodynamic polarizations were performed after 24 h exposure to the 0.05 M NaCl solutions with and without corrosion inhibitor. The samples, with a surface area of 3.14 cm^2, were polarized using a sweep rate of 1 mV/s and a sweep range of −200 to +200 mV versus the OCP. The anodic and cathodic polarizations were performed on separate samples starting from the OCP. The measurements were performed at least in triplicate for each anodic and cathodic polarization to ensure reproducibility.

2.1.2.3. Reversibility. The reversibility of the corrosion inhibitors was assessed with EIS. After the initial EIS measurement after 24 h exposure to 60 ml inhibitor solution, the inhibitor solution was removed, the electrochemical cell was 2 times gently rinsed with a 0.05 M NaCl solution to remove excess of corrosion inhibitor, and finally refilled with 60 ml 0.05 M NaCl solution. The EIS spectra were recorded as described above, directly and 24 h and 5 days after the removal of the corrosion inhibitor. For data analysis the impedance spectra were fitted with Zview from Scribner Associates Inc. using the appropriate equivalent circuits.

2.2. Active protective properties of inhibitor loaded coatings

2.2.1. Preparation of the organic model coatings

The corrosion inhibitors were incorporated into polyurethane model coatings to investigate the active protective properties. The formulations of the coatings are summarized in Table 1. The coatings were formulated to a total pigment volume concentration (PVC) of 30 vol%, this includes 5 vol% of corrosion inhibitor for the coatings loaded with 2-mercaptobenzothiazole (2-MBT-loaded), benzotriazole (BTA-loaded), and lithium carbonate (Li_2CO_3-loaded). The coating without corrosion inhibitor (Non-inhibited reference) contains 5 vol% of the inert barium sulphate instead of corrosion inhibitor.

Table 1
Composition of organic model coating.

	No inhibitor	2-MBT	BTA	Li_2CO_3
Component A				
N-Butylacetate	85.0 g	85.0 g	85.0 g	85.0 g
Desmophen 650MPA	47.7 g	47.7 g	47.7 g	47.7 g
2-MBT		7.2 g		
BTA			6.8 g	
Lithium carbonate				10.5 g
Magnesium oxide	16.4 g	16.4 g	16.4 g	16.4 g
Tioxide TR 92	5.2 g	5.2 g	5.2 g	5.2 g
Blanc Fixe N ($Ba(SO_4)$)	66.0 g	43.5 g	43.5 g	43.5 g
Component B				
Tolonate HDB 75 MX	28.5 g	28.5 g	28.5 g	28.5 g
Dynasilan Glymo	5.2 g	5.2 g	5.2 g	5.2 g

2.2.2. Sample preparation

The coatings were prepared by mixing the raw materials as follows: component A was prepared by adding the ingredients under stirring in a 370 ml glass jar. After the addition of 400 g Zirconox® pearls (1.7–2.4 mm), the pigments were dispersed to a fineness of grind less than 25 µm by shaking on a Skandex® paint shaker. After 20 min shaking, the pearls were separated from the coating. Component B was mixed separately and added to Component A just before application.

AA2024-T3 aluminium panels were anodized using tartaric sulphuric acid accordion to aerospace requirements (AIPI 02-01-003) resulting in an anodic film of 3–3.5 µm. The coating formulations were applied on these panels with a high volume low pressure (HVLP) spray gun. After the application at 23 °C and 55% RH, a 1 h flash-off period was applied followed by a force cure cycle of 1 h at 80 °C. The dry film thickness of the coatings after drying was 20–25 µm.

2.2.3. Inhibitor leaching

The leaching of the corrosion inhibitors from the organic coating matrix was investigated by immersing the coated samples with a surface area of 28 cm^2 in 50 ml deionized water. Prior to the immersion, the coatings were damaged with 20 parallel cuts with a length of 5 cm until the substrate using a razor blade achieving a total scribe length of 1 m to ensure sufficient leaching from the cut edges of the coating. Samples were taken every 10 min up to 1 h; further measurements were taken after 1.5 h, 2 h, 3 h, 4 h, and 6 h. The solutions of the exposed 2-MBT-loaded and BTA-loaded coatings were analysed with UV–vis spectroscopy (Agilent Cary 60 UV–vis spectrophotometer and the solutions obtained from the exposed Li_2CO_3-loaded coating were analysed with inductively coupled plasma atomic emission spectroscopy (Arcos NT ICP-AES). The samples for ICP-AES were acidified with nitric acid to a concentration of 0.1 M and measured using scandium as an internal standard.

2.2.4. Corrosion protection in the defect area

An artificial damage was made in the samples to investigate the active protective properties of these inhibitor-loaded coatings. The artificial defect, with a surface area of 0.48 cm^2, was prepared by mechanical milling resulting in two intersecting scribes with a length of 2 cm, width of 1 mm and depth of 100–150 µm. After scribing, the coated samples were exposed to the neutral salt spray test (NSS) according to ASTM-B117 for 7 days. After exposure, the defect area was evaluated by optical microscopy and the corrosion inhibitive properties were evaluated by EIS using the same equipment and settings as described above using a 0.05 M NaCl solution. In this case, the working electrode exposed to the electrolyte was the coating with the defect area. The total surface area of the electrochemical cell was of 12.5 cm^2 and the effective electrode (i.e. the coating defect) area was 0.48 cm^2. The impedance measurements were recorded after 5 h of exposure to the 0.05 M NaCl solution.

2.3. Inhibitor reversibility and inhibition efficiency

AA2024-T3 samples were mechanically ground with successive grades of SiC sanding paper up to 1200 grid using water as lubricant and then polished with 1 µm diamond paste. After polishing, the samples were cut into 1 cm^2 panels, ultrasonically cleaned in ethanol, dried at 40 °C and weighed with an analytical balance. The panels were immersed in 50 ml of 0.05 M NaCl solution with or without corrosion inhibitor (1 mM MBT, 5 mM BTA, 5 mM Li_2CO_3). One set of panels was exposed for 14 d to the corrosion inhibitor loaded solutions and another set of panels was exposed to the inhibitor solution for 24 h, followed by immersion in a 0.05 M NaCl solution without inhibitor (blank solution) for 13 d. Nitric acid is an effective desmutting agent and deoxidizer for aluminium and is a effective replacement for the toxic chromic acid desmutting method to dissolve the corrosion products from the aluminium panels [16,38]. After exposure to the solutions, all the panels (including the unexposed sample) were cleaned by immersion in a 1 M nitric acid solution for 2 h. After the cleaning procedure the panels were dried and weighed to determine the weight loss due to corrosion. The panels were visually examined with an optical microscope and the surface roughness of the sample (Sa (arithmetical mean height)) was measured with a Bruker K1 white light interferometer using a 20× objective. Sa expresses the surface roughness of an area, as an absolute value, the difference in height of each point compared to the arithmetical mean of the surface. This parameter is used to evaluate the roughness of surfaces [39,40]. For each sample a 4 × 4 mm area was measured and Vision for Profilers (version 4.2) software was used to analyse the data. All measurements were executed in duplicate. The inhibitor efficiency (IE) was determined from the weight loss measurements. First the corrosion rate (w) was calculated using Eq. (1) [41]:

$$w = \frac{m_{before} - m_{after}}{A.\ t} \quad (1)$$

Where m_{before} is the mass of the sample before exposure (mg) and m_{after} is the mass of the same coupon after the exposure. A is the area of the sample (mm^2) and t is the exposure time (h). With the corrosion rate value, IE was calculated using Eq. (2) [41]:

$$IE = \frac{w_o - w_{inh}}{w_o} X\ 100\% \quad (2)$$

In this equation, w_0 is the corrosion rate of the sample without corrosion inhibitor and w_{inh} is the corrosion rate of the sample in the presence of corrosion inhibitor in solution.

3. Results and discussion

3.1. Corrosion inhibition in an electrochemical cell

3.1.1. Potentiodynamic polarization measurements

Potentiodynamic polarization measurements were performed to investigate the corrosion inhibiting effect of the corrosion inhibitors on the anodic and cathodic electrode reactions. Fig. 1 shows the polarization curves after 24 h exposure of the AA2024-T3 samples to the inhibitor solutions. The sample without inhibitor shows immediate pitting when polarized anodically vs. the OCP and a diffusion limited cathodic polarization curve below $-0.58V_{SCE}$. The polarization curves of the samples that were exposed to the inhibitor solutions for 24 h, clearly demonstrate the inhibitive nature of the corrosion inhibitors. The corrosion potential of the aluminium samples that were exposed to the BTA and 2-MBT solutions shifted to less noble potentials and the cathodic currents were suppressed by about an order of magnitude. In addition to this, the anodic currents of these samples were reduced and the pitting potential shifted to more noble values of around $-0.51V_{SCE}$. The corrosion potential (E_{corr}) of the sample exposed to the Li_2CO_3 solution remained at $-0.54V_{SCE}$ and both the anodic and cathodic currents were suppressed. Table 2 summarizes the electrochemical parameters derived from the potentiodynamic polarization measurements displayed in Fig. 1. The corrosion current (i_{corr}) was approximated from the polarization resistance (R_{pol}) using the Stern-Geary equation. R_{pol} was obtained from the linear slope of the linear region ± 20 mV vs. E_{corr} [42,43].

From the results in Table 2, it can be noted that i_{corr} for the samples that were exposed to the inhibitor-loaded solutions was reduced by an order of magnitude as compared to that of the sample that was exposed to the blank solution. The 2-MBT solution provided the best corrosion protective properties on the AA2024-T3 samples with an i_{corr} of $3.96{\cdot}10^{-8}$ A/cm^2 and a R_{pol} 472 kΩ·cm^2 followed by the sample that was exposed to the BTA solution with an i_{corr} of $7.91{\cdot}10^{-8}$ A/cm^2 and a R_{pol} 215 kΩ cm^2. The i_{corr} of the sample exposed to the Li_2CO_3 solution was $3.08{\cdot}10^{-7}$ A/cm^2 and the R_{pol} 67 kΩ cm^2.

The cathodic branches of the potentiodynamic polarization curves

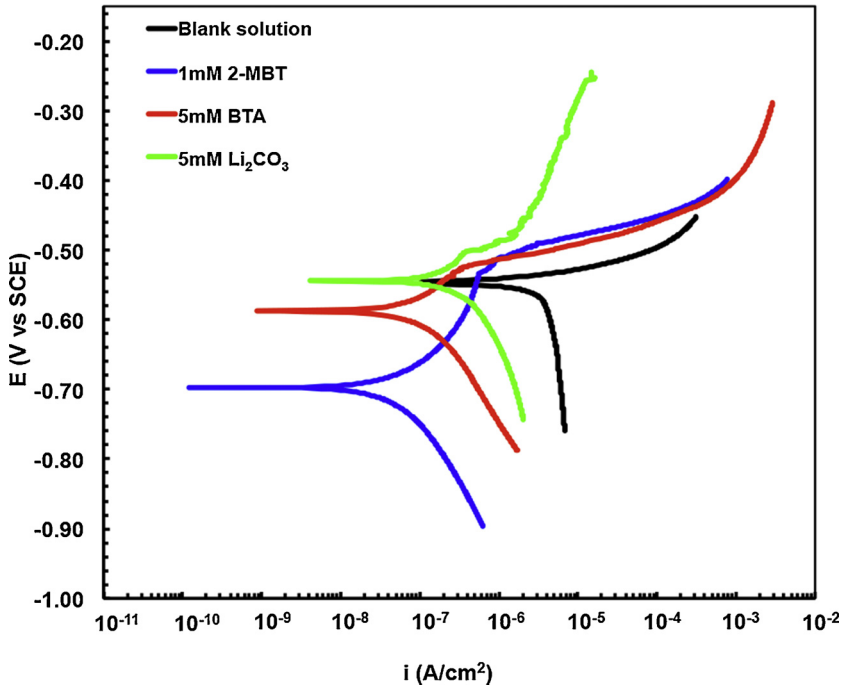

Fig. 1. Potentiodynamic polarization curves for AA2024-T3 aluminium alloy in 0.05 M NaCl with and without corrosion inhibitor.

Table 2
Electrochemical parameters obtained from the potentiodynamic polarization curves displayed in Fig. 1.

	E_{corr} (V_{SCE})	i_{corr} (A/cm^2)	R_{pol} ($k\Omega.cm^2$)	Passive range E_{pit}-E_{corr}(V)
Blank solution	−0.54	3.38×10^{-6}	3	0
1 mM 2-MBT	−0.70	3.96×10^{-8}	427	0.18
5 mM BTA	−0.59	7.91×10^{-8}	215	0.07
5 mM Li_2CO_3	−0.54	3.08×10^{-7}	67	0.05

show the diffusion limited reduction of the dissolved oxygen. The anodic branches show the passive ranges of the samples after 24 h exposure to the corrosion inhibitor solutions. The anodic polarization curves show a shift of the pitting potential (E_{pit}) to more noble values of all samples exposed to an inhibitor solution. The sample exposed to the 2-MBT solution showed the largest anodic passive range of 180 mV compared to 70 mV for the sample in the BTA solution. The sample exposed to the Li_2CO_3 solutions showed a relative small anodic passive range of 50 mV, followed by a slight increase of the anodic current density upon further anodic polarization. This indicates some limited anodic activity or pitting corrosion around 50 mV. However, the system did not progress to full pitting corrosion over the anodic polarization range of 200 mV. The anodic current density remained below 10^{-5} A cm^{-2}, two orders of magnitude lower than for the exposure to the organic corrosion inhibitor solutions at these potentials. This behaviour indicates that generated layer is covering the macroscopic surface area and is limiting the corrosion reactions and the breakdown potential of this layer exceeds the range of this anodic potentiodynamic polarization measurement. In general, exposure of AA2024-T3 to the tested inhibitor solutions provides improved corrosion protective properties resulting in increased R_{pol}, reduced i_{corr}, shifts in E_{corr} and the presence of passive ranges shifting E_{pit} to more noble potentials. These results imply that Li_2CO_3 and both organic corrosion inhibitors BTA and 2-MBT behave as mixed inhibitors providing anodic and cathodic inhibition as observed in earlier studies [13,15]. Based on the electrochemical parameters from these potentiodynamic polarizations (R_{pol}, i_{corr}, E_{corr} and the passive ranges) it can be concluded that the 2-MBT solution provides the most effective corrosion inhibition on AA2024-T3 followed by the BTA and Li_2CO_3 solutions.

3.1.2. Electrochemical impedance measurements

Further comparative analysis of the corrosion protective properties of the inhibitor solutions was performed with EIS. Fig. 2 shows the Bode plots after the exposure of AA2024-T3 to the 0.05 M NaCl solutions with and without corrosion inhibitor. The impedance modulus plot (Fig. 2a) shows that AA2024-T3 has the lowest impedance modulus value after 24 h exposure to the blank solution. The impedance modulus values increased when the alloy was exposed to the Li_2CO_3 solution. Exposure to the 2-MBT and BTA solutions resulted in an increase by more than an order of magnitude compared to the sample without inhibitor. This underlines the excellent intrinsic inhibitive properties of these organic corrosion inhibitors. The accompanying Bode phase angle plots are displayed in Fig. 2b. The phase angle plot of the sample exposed to the blank solution shows two time-constants, one for the oxide layer (middle frequency range 10^1–10^3 Hz) and the second for the electrochemical activity at the aluminium surface (low frequency range 10^{-2}-10^{-1} Hz). The phase angle plots of the samples exposed to the BTA and 2-MBT solutions show a typical impedance spectrum of a metal in an organic inhibitor electrolyte showing three time-constants. A time-constant in the low frequency range for the electrochemical processes at the aluminium substrate and two higher frequency range time-constants related to the oxide (10^{-1}–10^2 Hz) and organic inhibitor layer (10^1–10^3 Hz) on the substrate [13]. The phase angle plot of the sample that was exposed to the Li_2CO_3 solution shows also three time-constants that can be attributed to a generated corrosion protective layer on the alloy sample. One time-constant relates to the electrochemical processes in the low frequency range and two overlapping time-constants extending over the middle frequency range (10^{-1}–10^3 Hz) relate to a dense and porous oxide layer [34].

The results of these measurements have been fitted to compare corrosion protective properties of these inhibitor solutions on AA2024-T3. The fittings were performed with the equivalent circuits as shown in Fig. 3 derived from previous studies [13,34]. EC1 is a two time-constant equivalent circuit model to describe a sample that is exposed to the solution without corrosion inhibitor [13]. In this model, R_{sol} is the

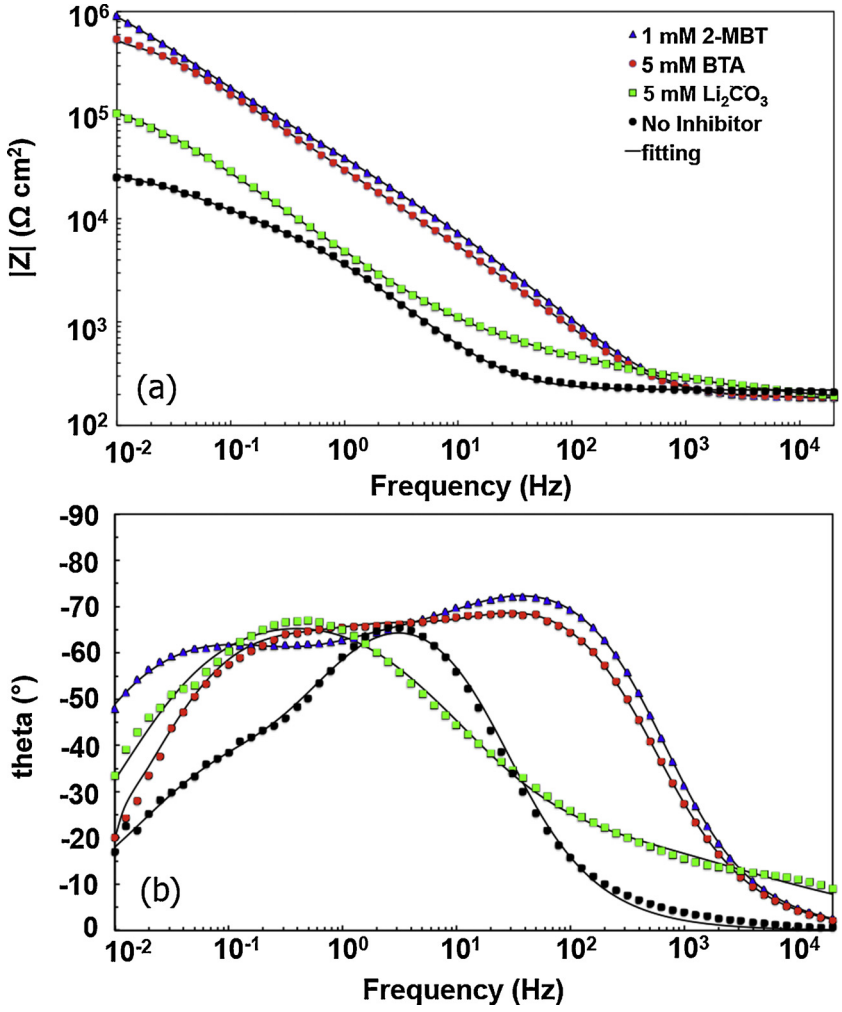

Fig. 2. Electrochemical impedance spectra of AA2024-T3 aluminium alloy after 24 h exposure to the 0.05 M NaCl solution with and without corrosion inhibitor. (a) impedance modulus and (b) phase angle.

solution resistance, and the first time-constant represents the resistance of the native aluminium oxide (R_{oxide}) and its capacitance properties (CPE_{oxide}). The second time-constant describes the electrochemical processes (corrosion) at the aluminium substrate in terms of the polarization resistance (R_{pol}) and the double layer capacitance (CPE_{dl}). Both, the organic inhibitors and Li_2CO_3 are represented by different equivalent circuits because their physical model of the corrosion protective layer is different [34]. EC2 describes the system when AA2024-T3 was exposed to the organic corrosion inhibitor solution (MBT or BTA) [13]. This EC features an additional time-constant describing the contribution of the resistance (R_{inh}) and capacitance (CPE_{inh}) of the corrosion-inhibiting layer that covers the copper-rich intermetallics [13].

Equivalent circuit EC3 is representative for the corrosion inhibiting layer covering the aluminium surface generated by exposing the aluminium alloy to a Li_2CO_3 solution [34]. In this system, the additional time-constant describes the contributions of the porous layer (R_{porous} and CPE_{porous}) on top of the dense oxide layer [34]. The fitted curves are displayed as solid lines in the Bode plots of Fig. 2. The quantitative data derived from these fittings are listed in Table 3. The constant phase elements (CPE) are used in these equivalent circuits to describe the elements with a non-ideal capacitive behaviour using parameter Q and n [44].

Although the inhibitors are described in different equivalent circuits, it is possible to compare the corrosion protective properties of these systems based on the oxide resistance (R_{oxide}) and polarization resistance (R_{pol}) values. In addition, the inhibitive layer resistance (R_{inh}) can be used to compare the properties of the corrosion inhibitive layer of both organic inhibitors. Table 3 reveals an additional stabilizing effect on the oxide layer by 2-MBT and BTA in addition to their corrosion inhibitive action as a result of the coverage of copper-rich intermetallic particles (R_{inh}). Compared to the sample that was exposed to the blank solution, R_{oxide} for the samples exposed to the 2-MBT and BTA solutions increased by a factor 15 to 19. This implies that 2-MBT and BTA have a stabilizing effect on the aluminium oxide as well, due to the adsorption of the inhibitor on the aluminium surface. This confirms the mixed anodic/cathodic inhibiting properties of these organic corrosion inhibitors observed with the potentiodynamic polarization measurements. R_{oxide} of the sample exposed to the Li_2CO_3 solution increased with a factor 4, which is significantly lower compared to the samples exposed to the BTA and 2-MBT solutions. A similar trend can be observed for R_{pol} of these samples, with estimated values of 2.16 MΩ·cm^2, 0.46 MΩ·cm^2 and 0.12 MΩ cm^2 for respectively the 2-MBT, BTA and Li_2CO_3 solutions. These EIS measurements and fittings show that the 2-MBT solution provides the best corrosion inhibitive properties on AA2024-T3 followed by the BTA and Li_2CO_3 solutions and confirm the findings and trends observed from the potentiodynamic polarization measurements.

3.2. Active protective properties in a coating

Inhibitor loaded coatings were formulated and their active

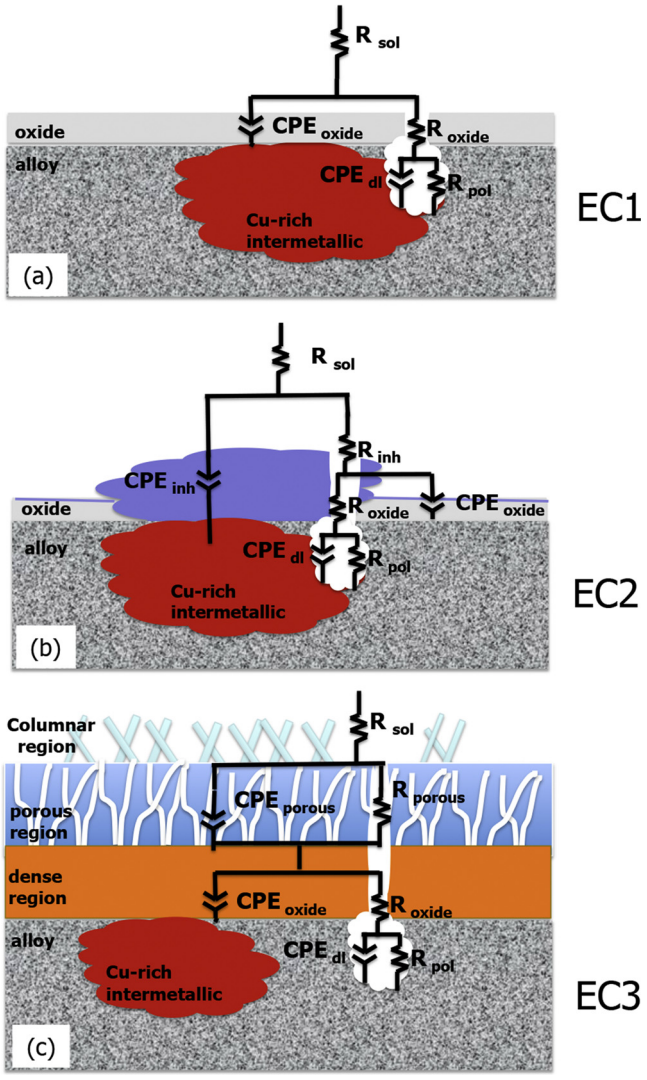

Fig. 3. Equivalent electric circuits used to fit the EIS spectra: (a) EC1 without inhibitor; (b) EC2 with organic inhibitor; (c) EC3 with Li_2CO_3.

protective properties were investigated in terms of leaching behaviour and the evaluation of the corrosion protective properties in an artificial defect after exposure to an accelerated corrosion test.

3.2.1. *Leaching of the corrosion inhibitors from the organic coating*

The leaching behaviour of the corrosion inhibitors from the organic model coatings is shown in Fig. 4. It shows the total released corrosion inhibitor as percentage of the total loading in the organic coating matrix during the first 6 h of immersion in deionized water at ambient conditions (23 °C and 55% RH). All three corrosion inhibitors show immediate leaching, but despite the equal loading in terms of volume (5% PVC) the leach rates differ significantly. The Li_2CO_3-loaded coating showed the fastest response of all inhibitors, leaching 2.5% of the active inhibitor in the first 30 min of exposure and 3.0% after 6 h. The 2-MBT-loaded coating showed a significantly slower leaching response compared to the Li_2CO_3-loaded coating with 0.7% after 30 min and increasing to 1.5% after 6 h followed by the BTA-loaded coating with the slowest leaching response of 0.3 and 0.5% after 30 min and 6 h respectively.

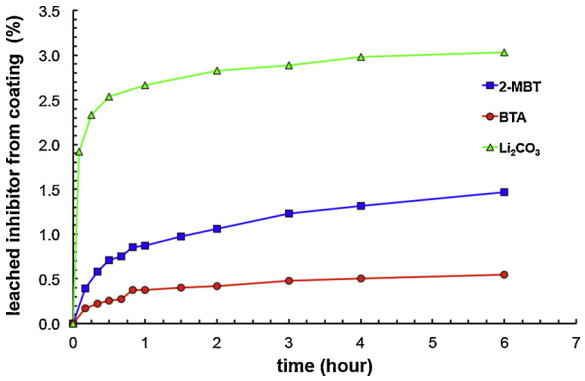

Fig. 4. Accumulated release of corrosion inhibitor from the organic coating matrix, normalized per cm2 model coating with a thickness of 25 µm over a 6 h time-period.

Based on the solubility parameters, it is logical to observe such a fast leaching for the Li_2CO_3-loaded coating. However, the slow leach rate of BTA from the organic coating suggests that BTA is less mobile in the coating matrix compared to 2-MBT. All samples show a similar leaching behaviour, an initial fast release related to the direct dissolution of the inhibitor at the coating/solution interface, followed by a slower leach rate after 1 h immersion. Inhibitor leaching is a complex process of dissolution and diffusion through the coating matrix. A non-Fickian leaching behaviour is often observed and this is assumed to be related to the diffusion/mass transport of the corrosion inhibitor from deeper in the coating matrix via interconnected pathways to the coating defect [45,46]. The leach rate is not only depending on the amount and solubility of the inhibitor, but it is also related to the pigment distribution and connectivity (microstructure) of the coatings [47,48]. The leach rate of the inhibitor from the coating and the irreversible reaction with the metal substrate are essential elements for effective active corrosion protection [49]. With the knowledge of the corrosion inhibiting and leaching properties of BTA, 2-MBT and Li_2CO_3, it can be assumed that these inhibitors can potentially provide active protection in a coating defect.

Table 3
Fitted parameters derived from the EIS measurements of AA2024-T3 in 0.05 M NaCl solution with and without corrosion inhibitor after 24 h exposure.

EC1		blank solution	EC2		1 mM 2-MBT	5 mM BTA	EC 3		5 mM Li_2CO_3
R_{sol}	Ωcm^2	220	R_{sol}	Ωcm^2	184	186	R_{sol}	Ωcm^2	157
			$Q(CPE_{inh})$	Ss^ncm^{-2}	2.80×10^{-6}	4.32×10^{-6}	$Q(CPE_{porous})$	Ss^ncm^{-2}	1.38×10^{-4}
			n_{inh}		0.9	0.88	n_{porous}		0.45
			R_{inh}	Ωcm^2	23791	18415	R_{Porous}	Ωcm^2	505
$Q(CPE_{Oxide})$	Ss^ncm^{-2}	$4{,}66 \times 10^{-5}$	$Q(CPE_{Oxide})$	Ss^ncm^{-2}	3.09×10^{-6}	2.79×10^{-6}	$Q(CPE_{Oxide})$	Ss^ncm^{-2}	4.89×10^{-5}
n_{oxide}		0.9	n_{oxide}		0.74	0.81	n_{oxide}		0.8
R_{oxide}	$k\Omega cm^2$	9	R_{oxide}	$k\Omega cm^2$	164	143	R_{oxide}	$k\Omega cm^2$	37
$Q(CPE_{dl})$	Ss^ncm^{-2}	1.46×10^{-4}	$Q(CPE_{dl})$	Ss^ncm^{-2}	2.89×10^{-6}	2.91×10^{-6}	$Q(CPE_{dl})$	Ss^ncm^{-2}	1.58×10^{-6}
n_{dl}		0.7	n_{dl}		0.76	0.82	n_{dl}		0.96
R_{pol}	$k\Omega cm^2$	23	R_{pol}	$k\Omega cm^2$	2162	462	R_{pol}	Ωcm^2	120
χ^2		4.29×10^{-3}	χ^2		5.81×10^{-5}	7.16×10^{-4}	χ^2		1.18×10^{-3}

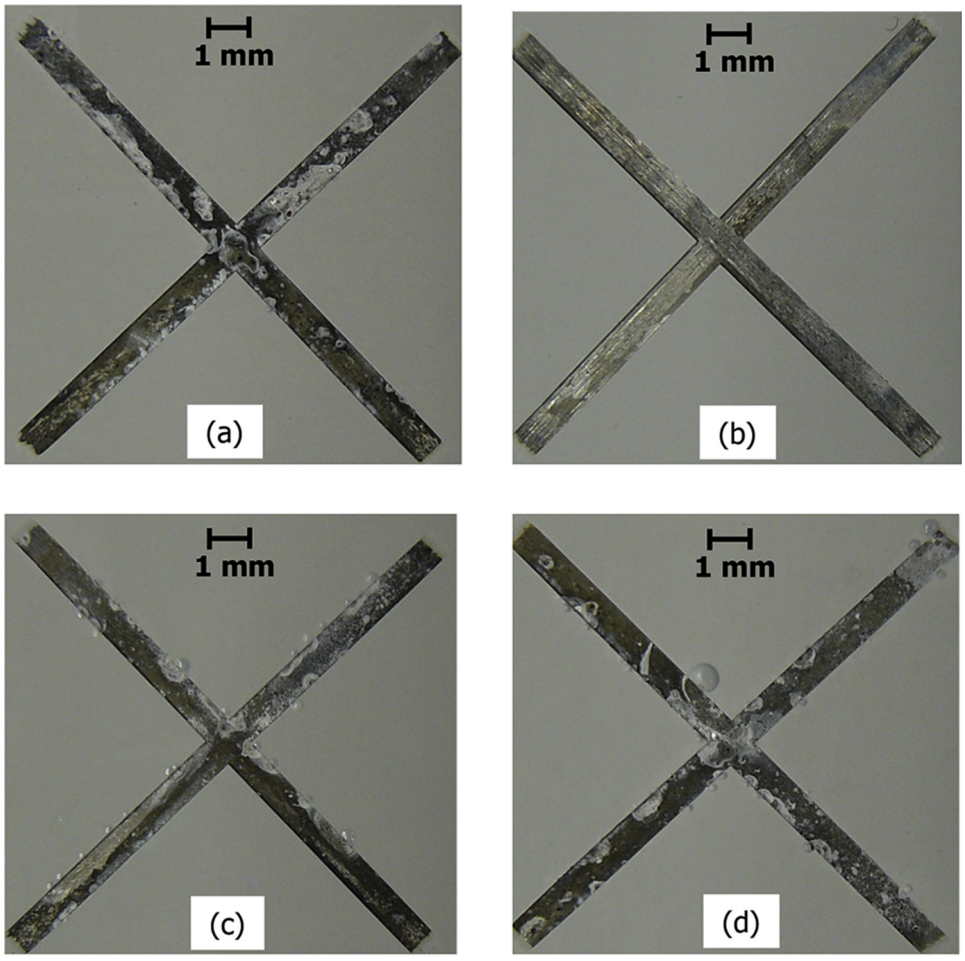

Fig. 5. Optical images of coated and scribed AA2024-T3 panels without and with leachable corrosion inhibitor after 168 h neutral salt spray exposure (ASTM B-117) (a) Non-inhibiting reference coating; (b) Li_2CO_3-loaded coating; (c) BTA-loaded coating, and (d) 2-MBT-loaded coating.

3.2.2. Visual evaluation of the active protective properties in a coating defect

The coatings loaded with and without leachable corrosion inhibitor were exposed to the neutral salt spray test (NSS) according to ASTM B-117 to assess the active protective properties of a coating in an artificial defect (scribe). Fig. 5 shows the appearance of the defect areas of the coatings assessed with an optical microscope after 168 h exposure to the NSS test. Despite the immediate leaching of corrosion inhibitor, as demonstrated in the previous section, the defect area of the BTA and 2-MBT loaded coatings do not show an improved corrosion protection compared to the non-inhibiting reference coating. Both samples showed darkening and white corrosion products in the defect area. In contrast to this, the defect area of the Li_2CO_3-loaded coating is free of corrosion products and retained a shiny appearance. This suggests that the lithium leaching coatings provided effective corrosion inhibition in the defect area.

3.2.3. Electrochemical properties of the coating defect

EIS can be used to evaluate the corrosion protective properties in a defect area as result of active protective activity of coatings [34]. Fig. 6 shows the EIS measurements of the defect areas acquired in a 0.05 M NaCl electrolyte after 168 h NSS exposure. The impedance modulus plot (Fig. 6a) reveals that the impedance of the Li_2CO_3 loaded coating is almost two to three times higher compared to the coatings loaded with BTA and MBT and the coating without corrosion inhibitor. The accompanying Bode phase angle plot (Fig. 6b) of the Li_2CO_3 loaded coating shows increased phase angle values and a broadened shape of the time-constant around 10^1–10^3 Hz which can be associated with a protective layer in the defect area [34].

The phase angle diagrams of the coatings loaded with BTA and 2-MBT are similar to the coating without a corrosion inhibitor. From these impedance measurements it is evident that the defect area of the coating sample loaded with Li_2CO_3 as leaching corrosion inhibitor shows an improved corrosion resistance compared to the samples without corrosion inhibitor or loaded with BTA or 2-MBT. These results suggest that despite the intrinsic corrosion inhibiting properties of BTA and 2-MBT and leaching characteristics from the organic coatings, both BTA and 2-MBT loaded coatings did not provide sufficient active corrosion protective properties to irreversibly passivate the aluminium surface in the coating defect under these conditions.

3.3. Inhibitor reversibility and efficiency

In order to explain the findings of the work summarized above, the reversibility and the inhibitor efficiency of these inhibitors were investigated using EIS, surface roughness and weight-loss measurements.

3.3.1. Electrochemical assessment of inhibitor reversibility

The reversibility of the corrosion inhibitors on AA2024-T3 was investigated by consecutive EIS measurements in the presence and after removal of the corrosion inhibitor solutions (Fig. 7). The EIS spectra were recorded with the inhibitor solution present and directly after replacement of the inhibitor solution by a 0.05 M NaCl solution (blank solution) and two additional measurements, 24 h and 5 d after replacement. Fig. 7a shows the EIS spectra for the AA2024-T3 exposed to the blank solution at the same time intervals. Fig. 7b–d show the EIS

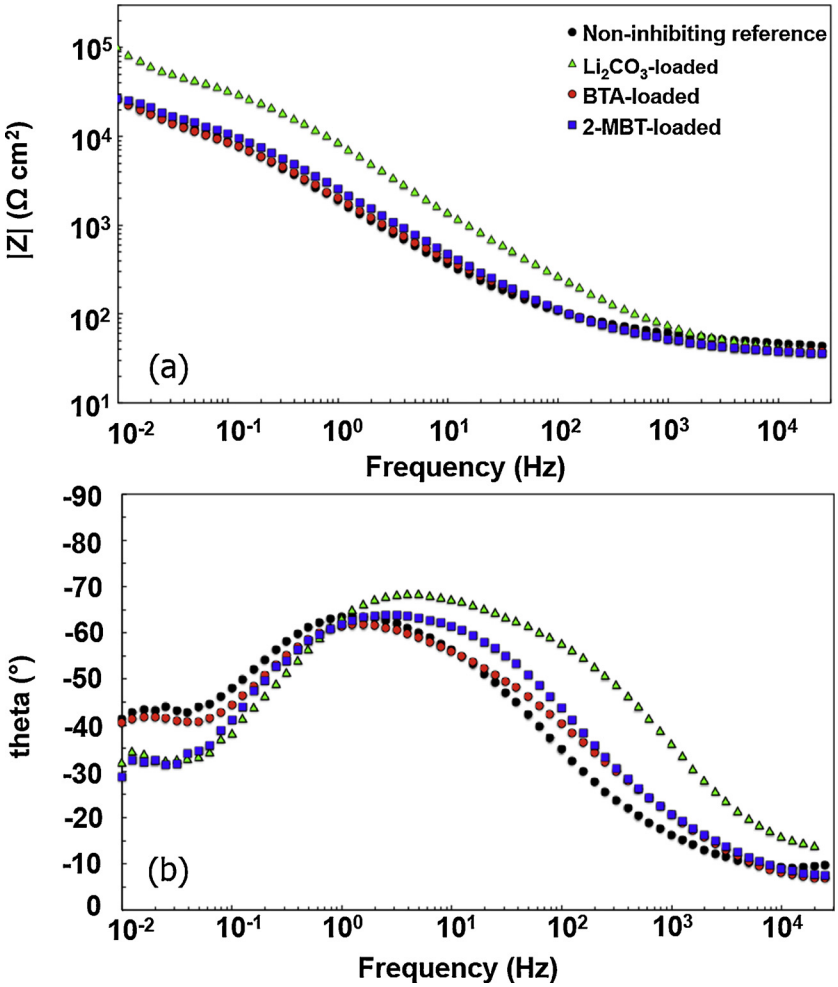

Fig. 6. Electrochemical impedance spectra of the defect areas of coatings loaded with and without leaching corrosion inhibitor on AA2024-T3 aluminium after 168 h NSS exposure measured in a 0.05 M NaCl solution: (a) impedance modulus (b) phase angle plot.

spectra of the samples before and after the replacement of the inhibitor solution. When the Li_2CO_3 solution was replaced by the blank solution (Fig. 7b), the impedance modulus decreased slightly over the entire frequency range. In the low frequency area (10^{-2} Hz) the impedance decreased from 65 kΩ cm^2 with the Li_2CO_3 solution present to 44 kΩ·cm^2 directly after replacement by the blank solution. However, this value increased again beyond the initial value to 93 kΩ cm^2 after 5 d exposure to the blank solution. The Bode phase angle plot showed an initial decrease of the middle frequency time-constant (10^1–10^3 Hz) followed by the broadening and increasing phase angle values of this time-constant, indicating further development of the oxide layer and its corrosion protective properties after the replacement of the inhibitor solution [49].

The BTA and 2-MBT solutions showed their characteristic effective corrosion inhibition on AA2024-T3 after 24 h exposure (Fig. 7c and d). However, the inhibitive nature of these inhibitors decreased significantly after the replacement of the inhibitor solution by the blank solution. The impedance modulus of the sample that was exposed to the BTA solution decreased directly by an order of magnitude over the entire frequency range after the replacement of the inhibitor solution by the blank solution. The impedance modulus decreased from 320 kΩ cm^2 to 26 kΩ cm^2 at 10^{-2} Hz, after the replacement of the BTA solution (Fig. 7c). When the 2-MBT solution was replaced by the blank solution, the impedance dropped at first only in the low frequency range (10^{-2} Hz) from 820 kΩ cm^2 to 400 kΩ cm^2 (Fig. 7d). However, longer exposures (up to 5 d) to the blank solution resulted in a further decrease of the impedance modulus to values equal to a sample that was exposed to the blank solution for 5 days. For both organic inhibitors, BTA and 2-MBT, this phenomenon is clearly visible in the Bode phase plot as well. The characteristic broad phase angle plot, observed for the samples exposed to the BTA or 2-MBT solution, disappears after the replacement with a blank solution. Finally, the phase angle plots have a similar appearance as the sample, which was exposed to the blank solution.

These EIS measurements were fitted with the equivalent circuits (EC1, EC2 and EC3) from Fig. 3 in order to compare the corrosion inhibitive properties of the corrosion inhibitors before and after their replacement with a blank solution. Fig. 8 shows the evaluation of the oxide resistance (R_{oxide}) and the oxide capacitance (C_{oxide}) and the polarization resistance (R_{pol}) and the double layer capacitance (C_{dl}) of the AA2024-T3 samples as a function of exposure time to the inhibited and non-inhibited solutions.

The equivalent capacitance (C) values used in these graphs were calculated from CPE values (n and Q) and the resistance (R) of the respective time-constant resulting from the fitting process using the equation derived by Hirschorn et al. (Eq. (3)) [50].

$$C = R^{\frac{(1-n)}{n}} \bullet Q^{\frac{1}{n}} \quad (3)$$

Fig. 8a shows the evolution of the oxide resistance (R_{oxide}) as a function of exposure time. The graph shows that R_{oxide} was relatively high for the samples exposed to the 2-MBT and BTA solutions with respective R_{oxide} values of 110 and 72 kΩ·cm^2. However, replacement of

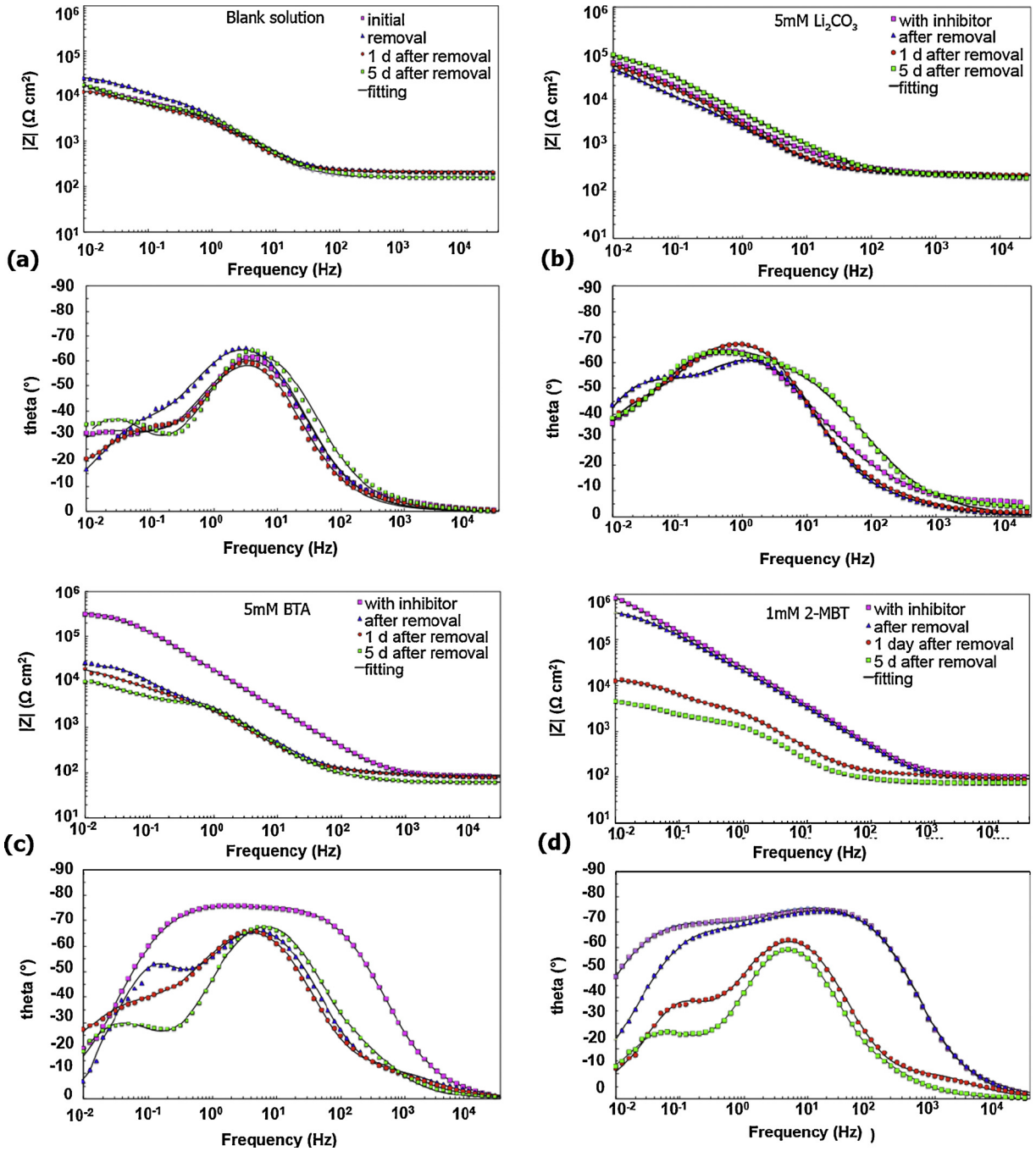

Fig. 7. Electrochemical impedance spectra of the corrosion inhibitors measured before and after their replacement by a blank solution (0.05 M NaCl) on AA2024-T3. Impedance modulus and phase angle plot (a) blank solution; (b) Li_2CO_3; (c) BTA, and (d) 2-MBT.

the inhibitor solution by the blank solution resulted in a decrease of R_{oxide} over time to values, around 5 kΩ cm^2, comparable to the sample that was exposed to the blank solution. In contrast to the organic corrosion inhibitors, the samples that were exposed to the Li_2CO_3 solution exhibited an increase of the oxide resistance up to 90 kΩ·cm^2 after the removal of the corrosion inhibitor. The capacitance values of the oxide layer (C_{oxide}) are shown in Fig. 8b. The C_{oxide} of the alloy was very low in the presence of the BTA and 2-MBT solutions, but C_{oxide} increased directly after replacing the inhibitor solutions by the blank solution. The C_{oxide} of the sample exposed to the Li_2CO_3 solution was the highest but decreased over time. These observations are in line with the decreasing R_{oxide} of the samples that were exposed to BTA and 2-MBT and the increasing R_{oxide} values for the sample exposed to the Li_2CO_3 solution. The rate of the corrosion process at the aluminium surface can be characterized by the polarization resistance (R_{pol}) [13]. Fig. 8b shows the development of R_{pol} before and after the removal of the inhibitor solutions. R_{pol} was relatively high for the samples when 2-MBT and BTA were present in the solution, respectively 1.1 and 0.7 MΩ·cm^2. However, the values for R_{pol} decreased significantly to 350 and 24 kΩ–cm^2 for 2-MBT and BTA respectively after the inhibitor solutions were replaced by the blank solution. The rapid decrease of R_{pol} of the sample exposed to the BTA solution confirms the stronger intrinsic inhibitive nature of 2-MBT [13]. R_{pol} of these samples decreased further upon extended exposure to values 15 kΩ cm^2, which is comparable to the sample, exposed to the blank solution after 24 and 5 d. The inset of Fig. 8c shows the development of R_{pol} of the samples that were exposed

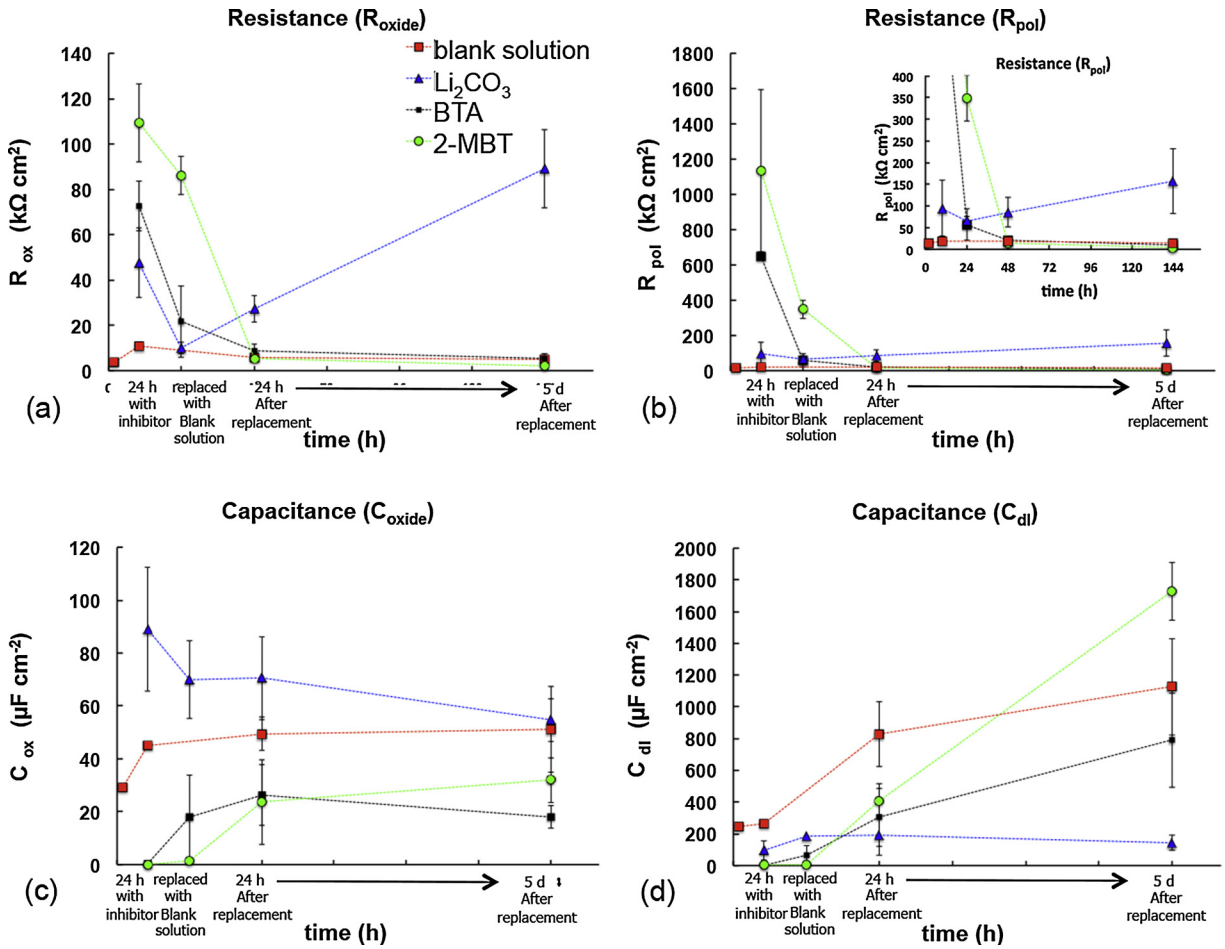

Fig. 8. Evolution of (a) the oxide resistance (Roxide), (b) polarization resistance(Rpol), (c) oxide capacitance (Coxide), and (d) double layer capacitance (Cdl) of aluminium alloys before and after removal of the corrosion inhibitor in 0.05 M NaCl solution. The inset of (b) shows a zoomed version of the graph.

to the Li_2CO_3 solution. R_{pol} was not as high (95 kΩ cm^2) in the presence of the Li_2CO_3 solution compared to the organic corrosion inhibitors, but after replacement by the blank solution, R_{pol} increased over time to 144 kΩ cm^2, indicating improving corrosion resistance with exposure time. The double layer capacitance (C_{dl}) displayed in Fig. 8d is related to the active corrosion area and hence can be linked with the corrosion activity of the samples [13]. After 24 h of exposure to the inhibitor solutions, all samples showed low double layer capacitance (C_{dl}) values combined with high R_{pol} values confirming the corrosion protective properties of these inhibitor solutions. After replacement of the inhibitor solutions by the blank solution, C_{dl} increased slightly for all samples. Whereas after extended exposure to the blank solution, the C_{dl} of the sample initially exposed to the Li_2CO_3 solution remained stable around 200 μF cm^{-2}, the C_{dl} of samples initially exposed to the 2-MBT and BTA solutions increased to respectively 1700 and 800 μF cm^{-2}. The increase of capacitance values (C_{oxide} and C_{dl}) combined with the simultaneous decrease of the resistance values (R_{oxide} and R_{pol}) are indicative for the degradation of the corrosion inhibitive properties for the samples initially exposed to the 2-MBT and BTA solutions. In contrast to this, the sample that was exposed to the Li_2CO_3 solution retained its corrosion protective properties after the removal of the Li_2CO_3 solution and even showed a further evolution of the oxide layer leading to higher R_{oxide} and R_{pol} values and lower C_{oxide} and C_{dl} values, thus improved corrosion protection. This increase implies that the protective layer densified after the replacement of the Li_2CO_3 by the blank solution. These results indicate that the corrosion inhibition mechanism of 2-MBT and BTA could be reversible processes.

3.3.2. *Surface roughness*

AA2024-T3 is susceptible to local corrosion phenomena such as pitting corrosion [4]. This results in increased surface roughness values when the surface of the alloy is corroding. The corrosion can be observed visually, but white light interferometer (WLI) profilometry measurements can provide a quantitative link with the degree of corrosion [51]. Fig. 9 shows the visual appearance of polished AA2024-T3 surfaces and the respective WLI surface maps before and after exposure to a 0.05 M NaCl solution with and without corrosion inhibitor. The optical image and WLI surface map of a pristine polished surface of AA2024-T3 before exposure are shown in Fig. 9a. However, the effects of corrosion, severe pitting corrosion, can be observed when the sample was exposed to the blank solution for 14 d (Fig. 9b). This was confirmed with the WLI surface map after removal of the corrosion products. The WLI surface map shows the variation in surface height in reference to the mean plane over the area of the sample. The mean plane is represented in green, lower areas are represented in blue shades and higher areas are displayed in red shades. The black areas are areas without information due to too deep pits or insufficient light reflection. Fig. 9c shows the performance when the AA2024-T3 panels were exposed for 14 d to the inhibitor solutions. The optical images and WLI maps show that the aluminium surface was almost not affected after the exposure. Fig. 9d shows the samples that were exposed to the blank solution after an initial exposure to the inhibitor solution. In contrast to the samples with inhibitor solution, both samples initially exposed to the BTA and 2-MBT solutions showed the effects of extensive pitting corrosion. On the other hand, the sample that was exposed to the

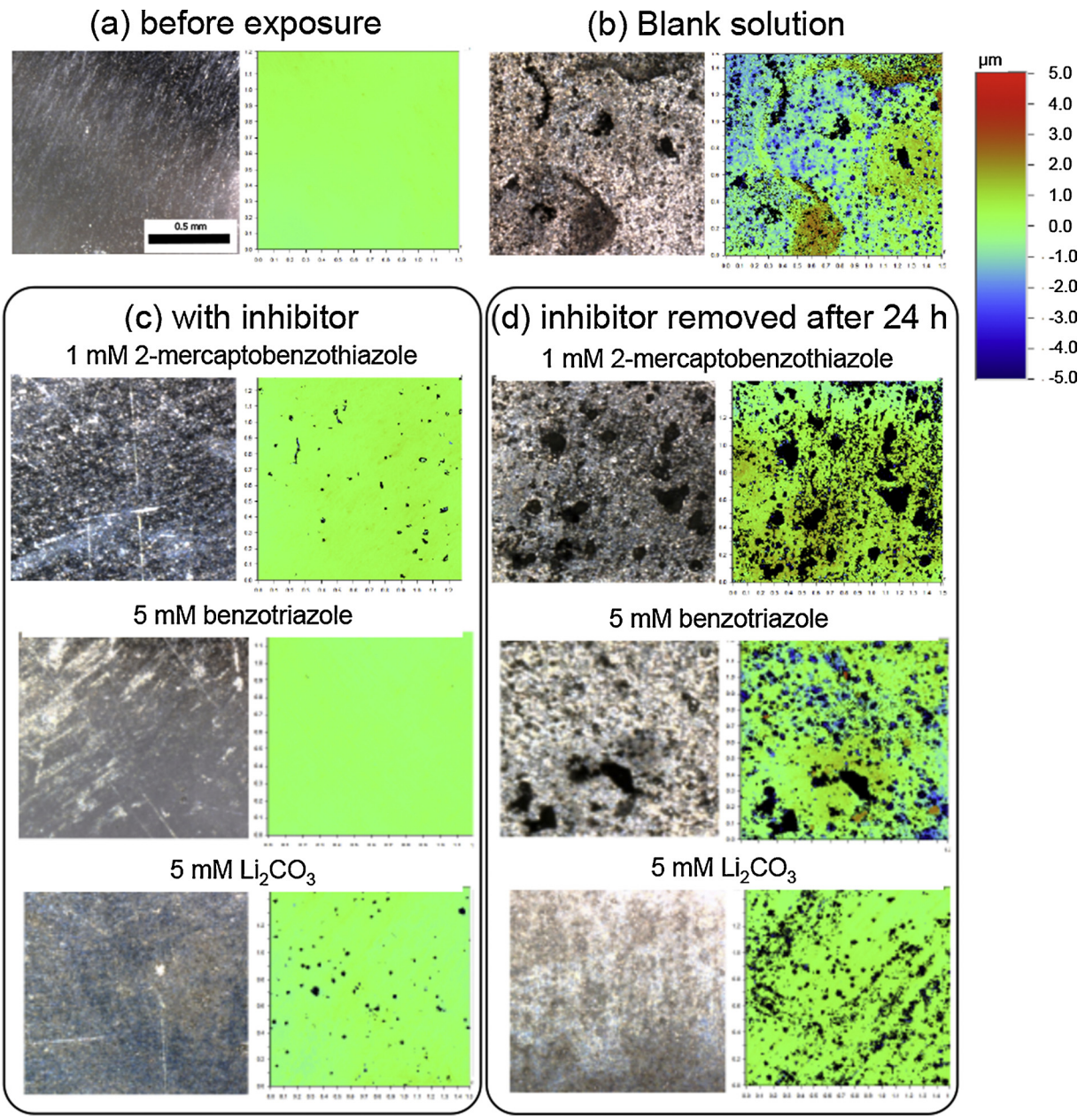

Fig. 9. Optical images and White light interferometer surface roughness maps of polished AA2024-T3 panels before and after exposure to 0.05 M NaCl solution, (a) before exposure; after (b) 14 d exposure without inhibitor; (c) 14 d exposure with corrosion inhibitor; (d) 14 d exposure but inhibitor removed after 24 h.

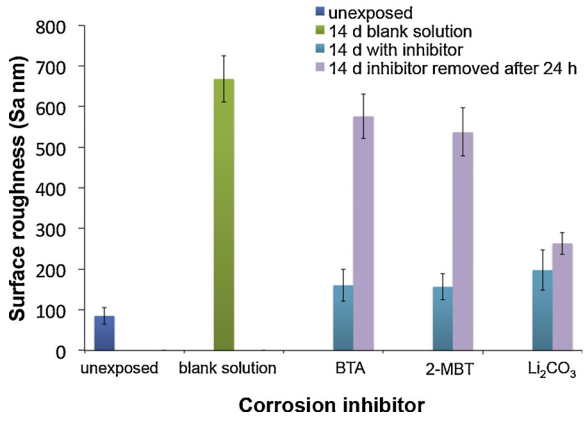

Fig. 10. Surface roughness (Sa) of the samples displayed in Fig. 9 derived from the white light interferometer surface maps.

Li_2CO_3 solution showed optically no signs of pitting corrosion and the WLI map showed only limited attack. Fig. 10 shows the quantitative surface roughness (S_a) results derived from the WLI measurements of the samples discussed above. The unexposed polished sample has an initial surface roughness around 80 nm, which increased due to corrosion to 670 nm after the 14 d exposure to the blank solution. This roughness excluded the deep pits (black areas) that could not be measured. More important, Fig. 10 shows the large increase of surface roughness of the samples after replacing the 2-MBT and BTA solutions by the blank solution. The surface roughness increased to values from 155 nm with 2-MBT present in the solution to 540 nm after replacement of the 2-MBT solution and 160 nm with BTA present in the solution to 570 nm after replacement of the BTA solution by the blank solution. The difference of the Li_2CO_3 exposed samples is significantly smaller, 200 nm for the sample exposed with inhibitor compared to 260 nm for the sample where Li_2CO_3 was replaced by the blank solution.

These optical observations and surface roughness measurements are

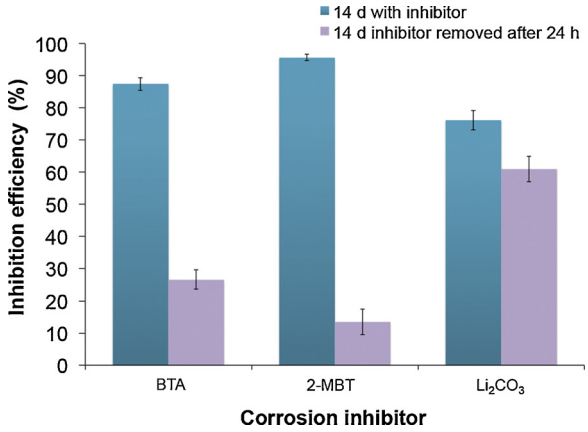

Fig. 11. Inhibitor efficiency of the corrosion inhibitors on AA2024-T3 after 14 d exposure to the solution with corrosion inhibitor and 14d exposure to a blank solution after removal of the corrosion inhibitor.

in line with the EIS observations and confirm the loss of protective properties of the AA2024-T samples when the BTA and 2-MBT solutions are replaced by a blank solution resulting in severe pitting corrosion and increase of surface roughness. In contrast to this, the sample exposed to the Li_2CO_3 inhibitor solution remained protected.

3.3.3. Inhibitor efficiency

The inhibitor efficiency (IE) of the inhibitors on AA2024-T3 was determined with and without replacement of the inhibitor solutions by a blank solution. Fig. 11 shows the IE of the corrosion inhibitors on AA2024-T3. Again, the excellent corrosion inhibitive nature of the BTA and 2-MBT inhibitor solutions on AA2024-T3 was demonstrated with an IE of 87% and 95% for BTA and 2-MBT, respectively. However, the IE decreased to respectively 26% and 14% when the inhibitor solution was replaced by a blank solution after 24 h. The IE of the sample in the presence of the Li_2CO_3 solution was 76% and 61% after replacement of the Li_2CO_3 solution by the blank solution. It has to be considered that the corrosion protective mechanism of Li_2CO_3 on aluminium involves dissolution of aluminium from the substrate due to anodic dissolution to generate an aluminium oxide/hydroxide layer [33]. This layer will be removed in the acidic cleaning procedure prior to the IE assessment. This results in relative lower IE values compared to the organic inhibitors. However, the results of the study still clearly demonstrate that the BTA and 2-MBT are only effective as corrosion inhibitors on AA2024-T3 when present in the solution. Moreover, it can be concluded that the IE of Li_2CO_3 is not as high as the organic inhibitors when the inhibitors are present in the solution but Li_2CO_3 clearly outperforms the organic corrosion inhibitors when the inhibitors are removed after 24 h and the exposure to corrosive conditions are continued.

3.4. Mechanistic difference of the inhibitors

The results of this work demonstrate that there is a significant difference in the corrosion inhibition mechanism of organic corrosion inhibitors such as BTA and 2-MBT compared to Li_2CO_3. The investigations demonstrate that the organic inhibitors were active in an electrochemical cell but showed very little active corrosion protection when incorporated as leachable corrosion inhibitor into a coating. The difference of the corrosion inhibitive mechanism of BTA and 2-MBT compared to Li_2CO_3 is schematically shown in Fig. 12. Organic inhibitors such as 2-MBT or BTA are very well known for their effective inhibition of AA2024-T3 aluminium alloys due to their nature to complex with the copper-rich intermetallic particles and predominantly reduce the cathodic oxygen reduction reaction. However measurements revealed that these inhibitors provide some anodic inhibition as well. This anodic inhibition can be attributed to the adsorption of the organic inhibitors to the aluminium surface [15]. Although the electrochemical and inhibitor efficiency experiments demonstrated that when the BTA and 2-MBT solutions were replaced by a blank solution the exposed AA2024-T3 showed rather low corrosion resistance. This suggests that the adsorption of these organic inhibitors on the copper-rich intermetallic particles and aluminium alloy are not permanent and that the physically adsorbed inhibitor molecules desorb when the inhibitor concentration diminishes. This would suggest that BTA and 2-MBT are intrinsically reversible corrosion inhibitors (Fig. 12a).

Over the years, BTA and 2-MBT have been used in a variety of studies for (active) corrosion protection However, none of these approaches demonstrated to perform equally or better as chromates nor have been authorized as a suitable alternative in the aerospace industry [2,52]. Therefore, it can be postulated that these effective organic inhibitors do not meet the criteria for active corrosion protection from coatings, being: soluble and provide fast, effective, and irreversible inhibition alike chromates [3]. These results imply that organic corrosion inhibitors such as BTA and 2-MBT might not be suitable for all applications of active protective coatings and may only be used in confined spaces where the concentration of corrosion inhibitor can be maintained at a sufficient high level.

Li_2CO_3 is known for its property to passivate aluminium by the formation of a protective layer on the aluminium substrate [53,54]. The corrosion protective properties of the samples exposed to the Li_2CO_3 solution may be not as high as the organic inhibitors but the accelerated exposure tests, electrochemical evaluations and inhibitor efficiency experiments clearly demonstrated the corrosion inhibiting effect of Li_2CO_3 on AA2024-T3. More important, the sample maintained its protective properties after the concentration of Li_2CO_3 decreased and demonstrating an irreversible nature of the protective layer that is formed on the aluminium alloy (Fig. 10b). Considering the criteria for corrosion inhibitors to be used in active protective coatings: soluble in water combined with fast, effective and irreversible inhibition, it can be concluded that Li_2CO_3 demonstrated all these properties. As such, this investigation demonstrates that Li_2CO_3 exhibits a unique mode of active corrosion protection that has not been demonstrated by any other environmentally friendly leaching corrosion inhibitor for the protection of high strength aluminium alloys.

4. Conclusions

This work compared the active protective properties (solubility, inhibition and reversibility) of Li_2CO_3 and the organic inhibitors, BTA and 2-MBT on AA2024-T3. In an electrochemical cell, all corrosion inhibitors demonstrated effective corrosion inhibition on AA2024-T3: 2-MBT > BTA > Li_2CO_3.

When incorporated in an organic coating, all inhibitors were able to leach from the coating. However, only the Li_2CO_3 loaded coating demonstrated effective corrosion protection in the artificial defect area exposed to the NSS accelerated corrosion test. Electrochemical analysis and inhibitor efficiency studies demonstrated that both organic corrosion inhibitors BTA and 2-MBT exhibit a reversible nature resulting in severe corrosion of the aluminium alloy when the inhibitor concentration diminishes.

Li_2CO_3 demonstrated that it is able to provide all characteristics of what is expected of corrosion inhibitors for active protective coatings: leaching, fast, effective and irreversible corrosion inhibition. The results of this study provide more insight into the unique properties of the active corrosion protective nature of the lithium-leaching coating technology for the protection of aluminium alloys.

Conflicts of interest

The authors declare no conflict of interest.

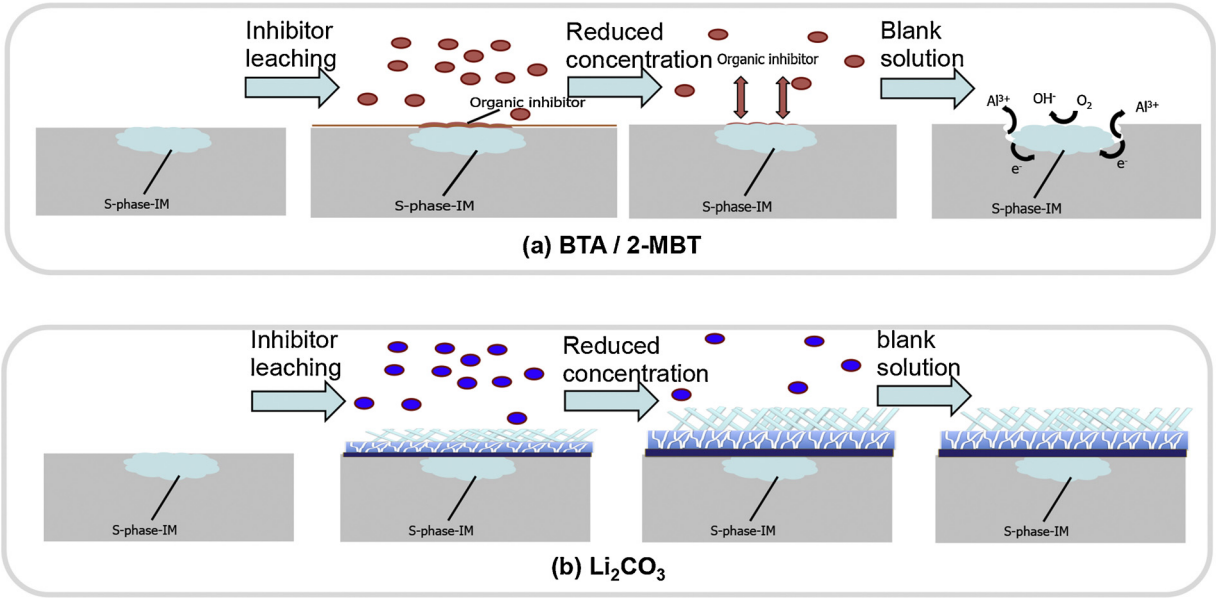

Fig. 12. Schematic illustration of the corrosion inhibiting mechanism of (a) organic corrosion inhibitors and (b) Li_2CO_3 as leachable inhibitor.

Acknowledgements

The authors would like to acknowledge Zeynep Devecioglu for her explorative work, Patrick van Holst and Harry Jansen of the department of precision and microsystems engineering (PME) for the access to the white light interferometer, Derek Graham and the analytical team of AkzoNobel Specialty Chemicals for their assistance with the reversibility and leaching experiments This research was carried out under the collaboration agreement between AkzoNobel and Delft University of Technology.

References

[1] A.K. Chattopadhyay, M.K.R. Zentner, Aerospace and aircraft coatings, Fed. Soc. For. Coat. Technol. (1990).
[2] J. Sinko, Challenges of chromate inhibitor pigments replacement in organic coatings, Prog. Org. Coat. 42 (2001) 267–282.
[3] M.W. Kendig, R.G. Buchheit, Corrosion inhibition of aluminum and aluminum alloys by soluble chromates, chromate coatings, and chromate-free coatings, Corrosion 59 (2003) 379–400.
[4] R.G. Buchheit, R.P. Grant, P.F. Hlava, B. McKenzie, G.L. Zender, Local dissolution phenomena associated with S phase (Al2CuMg) particles in aluminum alloy 2024-T3, J. Electrochem. Soc. 144 (1997) 2621–2628.
[5] A.E. Hughes, N. Birbilis, J.M.C. Mol, J. Santiago, S.J. Garcia, X. Zhou, G.E. Thompson, High strength Al-alloys: microstructure, corrosion and principles of protection, in: P.Z. Ahmad (Ed.), Recent Trends in Processing and Degradation of Aluminium Alloys, In Tech, 2011.
[6] A. Boag, R.J. Taylor, T.H. Muster, N. Goodman, D. McCulloch, C. Ryan, B. Rout, D. Jamieson, A.E. Hughes, Stable pit formation on AA2024-T3 in a NaCl environment, Corros. Sci. 52 (2010) 90–103.
[7] P. Leblanc, G.S. Frankel, A study of corrosion and pitting initiation of AA2024-T3 using atomic force microscopy, J. Electrochem. Soc. 149 (2002) B239–B247.
[8] M. Kendig, S. Jeanjaquet, Cr(VI) and Ce(III) inhibition of oxygen reduction on copper, J. Electrochem. Soc. 149 (2002) B47–B51.
[9] K. Xhanari, M. Finšgar, Organic corrosion inhibitors for aluminum and its alloys in chloride and alkaline solutions: a review, Arab. J. Chem. (2016).
[10] M. Metikos-Hukovic, R. Babic, A. Marinovic, Spectrochemical characterization of benzotriazole on copper, J. Electrochem. Soc. 145 (1998) 4045–4051.
[11] M. Ohsawa, W. Suetaka, Spectro-electrochemical studies of the corrosion inhibition of copper by mercaptobenzothiazole, Corros. Sci. 19 (1979) 709–722.
[12] G. Williams, A.J. Coleman, H.N. McMurray, Inhibition of aluminium alloy AA2024-T3 pitting corrosion by copper complexing compounds, Electrochim. Acta 55 (2010) 5947–5958.
[13] M.L. Zheludkevich, K.A. Yasakau, S.K. Poznyak, M.G.S. Ferreira, Triazole and thiazole derivatives as corrosion inhibitors for AA2024 aluminium alloy, Corros. Sci. 47 (2005) 3368–3383.
[14] M.M. Antonijevic, M.B. Petrovic, Copper corrosion inhibitors. A review, Int. J. Electrochem. Sci. 3 (2008) 1–28.
[15] I. Recloux, F. Andreatta, M.-E. Druart, L.B. Coelho, C. Cepek, D. Cossement, L. Fedrizzi, M.-G. Olivier, Stability of benzotriazole-based films against AA2024 aluminium alloy corrosion process in neutral chloride electrolyte, J. Alloys Compd. 735 (2018) 2512–2522.
[16] T.G. Harvey, S.G. Hardin, A.E. Hughes, T.H. Muster, P.A. White, T.A. Markley, P.A. Corrigan, J. Mardel, S.J. Garcia, J.M.C. Mol, A.M. Glenn, The effect of inhibitor structure on the corrosion of AA2024 and AA7075, Corros. Sci. 53 (2011) 2184–2190.
[17] A.C. Balaskas, M. Curioni, G.E. Thompson, Effectiveness of 2-mercaptobenzothiazole, 8-hydroxyquinoline and benzotriazole as corrosion inhibitors on AA 2024-T3 assessed by electrochemical methods, Surf. Interface Anal. 47 (2015) 1029–1039.
[18] L.B. Coelho, D. Cossement, M.G. Olivier, Benzotriazole and cerium chloride as corrosion inhibitors for AA2024-T3: an EIS investigation supported by SVET and ToF-SIMS analysis, Corros. Sci. 130 (2018) 177–189.
[19] S. Marcelin, N. Pebere, Synergistic effect between 8-hydroxyquinoline and benzotriazole for the corrosion protection of 2024 aluminium alloy: a local electrochemical impedance approach, Corros. Sci. 101 (2015) 66–74.
[20] S.V. Lamaka, M.L. Zheludkevich, K.A. Yasakau, M.F. Montemor, P. Cecilio, M.G.S. Ferreira, TiOx self-assembled networks prepared by templating approach as nanostructured reservoirs for self-healing anticorrosion pre-treatments, Electrochem. Commun. 8 (2006) 421–428.
[21] A. Shanaghi, M. Kadkhodaie, Investigation of high concentration of benzotriazole on corrosion behaviour of titania-benzotriazole hybrid nanostructured coating applied on Al 7075 by the sol-gel method, Corr. Eng. Sci. Technol. 52 (2017) 332–342.
[22] I. Recloux, Y. Gonzalez-Garcia, M.E. Druart, F. Khelifa, P. Dubois, J.M.C. Mol, M.G. Olivier, Active and passive protection of AA2024-T3 by a hybrid inhibitor doped mesoporous sol–gel and top coating system, Surf. Coat. Technol. 303 (2016) 352–361.
[23] D.G. Shchukin, M. Zheludkevich, K. Yasakau, S. Lamaka, M.G.S. Ferreira, H. Mohwald, Layer-by-layer assembled nanocontainers for self-healing corrosion protection, Adv. Mater. 18 (2006) 1672-+.
[24] M. Parsa, S.M.A. Hosseini, Z. Hassani, E. Jamalizadeh, Corrosion protective properties of coatings doped with inhibitors, Anti-Corros. Method Mater. 61 (2014) 416–422.
[25] M.L. Zheludkevich, D.G. Shchukin, K.A. Yasakau, H. Mohwald, M.G.S. Ferreira, Anticorrosion coatings with self-healing effect based on nanocontainers impregnated with corrosion inhibitor, Chem. Mater. 19 (2007) 402–411.
[26] J. Carneiro, A.F. Caetano, A. Kuznetsova, F. Maia, A.N. Salak, J. Tedim, N. Scharnagl, M.L. Zheludkevich, M.G.S. Ferreira, Polyelectrolyte-modified layered double hydroxide nanocontainers as vehicles for combined inhibitors, RSC Adv. 5 (2015) 39916–39929.
[27] F. Maia, J. Tedim, A.D. Lisenkov, A.N. Salak, M.L. Zheludkevich, M.G.S. Ferreira, Silica nanocontainers for active corrosion protection, Nanoscale 4 (2012) 1287–1298.
[28] A.C. Balaskas, T. Hashimoto, M. Curioni, G.E. Thompson, Two-shell structured PMAA@CeO2 nanocontainers loaded with 2-mercaptobenzothiazole for corrosion protection of damaged epoxy coated AA 2024-T3, Nanoscale 9 (2017) 5499–5508.
[29] F. Maia, K.A. Yasakau, J. Carneiro, S. Kallip, J. Tedim, T. Henriques, A. Cabral, J. Venancio, M.L. Zheludkevich, M.G.S. Ferreira, Corrosion protection of AA2024 by sol-gel coatings modified with MBT-loaded polyurea microcapsules, Chem. Eng. J. 283 (2016) 1108–1117.
[30] P. Visser, Y. Liu, X. Zhou, T. Hashimoto, G.E. Thompson, S.B. Lyon, L.G.J. van der Ven, A.J.M.C. Mol, H.A. Terryn, The corrosion protection of AA2024-T3 aluminium alloy by leaching of lithium-containing salts from organic coatings, Faraday Discuss. 180 (2015) 511–526.
[31] P. Visser, Y. Liu, H. Terryn, J.M.C. Mol, Lithium salts as leachable corrosion

inhibitors and potential replacement for hexavalent chromium in organic coatings for the protection of aluminum alloys, J. Coat. Technol. Res. 13 (2016) 557–566.
[32] P. Visser, A. Lutz, J.M.C. Mol, H. Terryn, Study of the formation of a protective layer in a defect from lithium-leaching organic coatings, Prog. Org. Coat. 99 (2016) 80–90.
[33] P. Visser, Y. Gonzalez-Garcia, J.M.C. Mol, H. Terryn, Mechanism of passive layer formation on AA2024-T3 from alkaline lithium carbonate solutions in the presence of sodium chloride, J. Electrochem. Soc. 165 (2018) C60–C70.
[34] P. Visser, M. Meeusen, Y. Gonzalez-Garcia, H. Terryn, J.M.C. Mol, Electrochemical evaluation of corrosion inhibiting layers formed in a defect from lithium-leaching organic coatings, J. Electrochem. Soc. 164 (2017) C396–C406.
[35] 2 -Mercaptobenzothiazol (2-(3H)-Benzothiazolthion) [MAK Value Documentation in German language, 1999], in: The MAK-Collection for Occupational Health and Safety, Wiley-VCH Verlag GmbH & Co. KGaA, 2002.
[36] 1H-Benzotriazole [MAK Value Documentation, 1991], in: The MAK-Collection for Occupational Health and Safety, Wiley-VCH Verlag GmbH & Co. KGaA, 2002.
[37] D. Wright, M.C. McMills, Lithium carbonate, Encyclopedia of Reagents for Organic Synthesis, John Wiley & Sons, Ltd, 2001.
[38] U. Tiringer, J. Kovač, I. Milošev, Effects of mechanical and chemical pre-treatments on the morphology and composition of surfaces of aluminium alloys 7075-T6 and 2024-T3, Corros. Sci. 119 (2017) 46–59.
[39] L. Deck, P. de Groot, High-speed noncontact profiler based on scanning white-light interferometry, Appl. Opt. 33 (1994) 7334–7338.
[40] U.C. Nwaogu, N.S. Tiedje, H.N. Hansen, A non-contact 3D method to characterize the surface roughness of castings, J. Mater. Process. Technol. 213 (2013) 59–68.
[41] M. Behpour, S.M. Ghoreishi, N. Mohammadi, N. Soltani, M. Salavati-Niasari, Investigation of some Schiff base compounds containing disulfide bond as HCl corrosion inhibitors for mild steel, Corros. Sci. 52 (2010) 4046–4057.
[42] M. Stern, A.L. Geary, Electrochemical polarization: I. A theoretical analysis of the shape of polarization curves, J. Electrochem. Soc. 104 (1957) 56–63.
[43] T.A. Zawodzinski, JES Classics, Electrochemical Society Interface, (2009), p. 59.
[44] C.H. Hsu, F. Mansfeld, Concerning the conversion of the constant phase element parameter Yo into a capacitance, Corrosion 57 (2001) 747.
[45] T. Prosek, D. Thierry, A model for the release of chromate from organic coatings, Prog. Org. Coat. 49 (2004) 209–217.
[46] F.H. Scholes, S.A. Furman, A.E. Hughes, T. Nikpour, N. Wright, P.R. Curtis, C.M. Macrae, S. Intem, A.J. Hill, Chromate leaching from inhibited primers. Part I. Characterisation of leaching, Prog. Org. Coat. 56 (2006) 23–32.
[47] S.G.R. Emad, X. Zhou, S.B. Lyon, G.E. Thompson, Y. Liu, G. Smyth, D. Graham, D. Francis, S.R. Gibbon, Influence of volume concentration of active inhibitor on microstructure and leaching behaviour of a model primer, Prog. Org. Coat. 102 (2017) 71–81.
[48] A.E. Hughes, A. Trinchi, F.F. Chen, Y.S. Yang, I.S. Cole, S. Sellaiyan, J. Carr, P.D. Lee, G.E. Thompson, T.Q. Xiao, The application of multiscale quasi 4D CT to the study of SrCrO4 distributions and the development of porous networks in epoxy-based primer coatings, Prog. Org. Coat. 77 (2014) 1946–1956.
[49] R. Oltra, F. Peltier, Influence of mass transport on the competition between corrosion and passivation by inhibitor release after coating breakdown, Prog. Org. Coat. 92 (2016) 44–53.
[50] B. Hirschorn, M.E. Orazem, B. Tribollet, V. Vivier, I. Frateur, M. Musiani, Determination of effective capacitance and film thickness from constant-phase-element parameters, Electrochim. Acta 55 (2010) 6218–6227.
[51] P. Visser, Novel totally chrome free corrosion inhibiting coating technology for protection of aluminium alloys, Trans. Inst. Met. Finish. 89 (2011) 291–294.
[52] R.L. Twite, G.P. Bierwagen, Review of alternatives to chromate for corrosion protection of aluminum aerospace alloys, Prog. Org. Coat. 33 (1998) 91–100.
[53] J. Gui, T.M. Devine, Influence of lithium on the corrosion of aluminum, Scripta Metallurgica 21 (1987) 853–857.
[54] R.G. Buchheit, M.D. Bode, G.E. Stoner, Corrosion-resistant, chromate free talc coatings for aluminum, Corrosion 50 (1994) 205–214.